The Role of Hydrogen Bonding in Supercooled Methanol

Ricardo Palomar and Gemma Sesé*

Departament de Física i Enginyeria Nuclear, Universitat Politècnica de Catalunya, Campus Nord-Mòdul B4, c/Jordi Girona 1-3, 08034 Barcelona, Spain

Received: July 6, 2004; In Final Form: October 28, 2004

The role of hydrogen bonding on the microscopic properties of supercooled methanol has been analyzed by means of molecular dynamics simulations. Thermodynamic, structural, and dynamical properties have been investigated in supercooled methanol. The results have been compared with those of an ideal methanol-like system whose molecules have the same dipole moment as the methanol but lack sites for hydrogen bonding. Upon cooling the methanol samples, translational relaxation times increase more rapidly than reorientational ones. This effect is much more important when hydrogen bonds are suppressed. Suppression of hydrogen bonds also results in lower critical temperatures for diffusion and for several characteristic relaxation time constants. The anisotropy of individual dynamics and the existence of dynamical heterogeneities have also been investigated.

1. Introduction

The study of supercooled liquids is a challenging area in statistical physics, as the microscopic mechanisms leading to the slowing down of the dynamics at temperatures close to the glass transition are not completely understood. Simulation has strongly contributed to the present knowledge of the supercooled state. It has been used extensively in the study of monatomic and binary mixtures[1] and also in the study of some molecular liquids, such as *o*-terphenyl,[2] water,[3] and ethanol.[4] Some of the predictions of the mode-coupling theory (MCT)[5,6,7] have been confirmed by these computer experiments. Nevertheless, simulation allows one to perform not only realistic studies but also analyses that are not feasible in real experiments. In a simulation, it is possible to check, for instance, the influence of the parameters used to model a system on a specific property. As an example, it has been observed that the long-term dynamics is not influenced by the underlying microscopic dynamics in a supercooled binary Lennard-Jones mixture.[8] For a similar system, the issue of the influence of the potential parameters on the fragility and other properties such as relaxation times has also been addressed.[9] Simulation might also help to analyze whether the microscopic details defining a liquid might influence the behavior of a system upon cooling, its translational and reorientational motions, and the existence of a spatially heterogeneous dynamics, which has been experimentally proven in some systems.[10]

Alcohols are glass-forming liquids which display exceptional behavior upon cooling. The temperature dependence of the viscosity of alcohols shows moderate deviations from an Arrhenius law, which would allow one to classify them as liquids of intermediate fragility. Nevertheless, their specific heat changes abruptly upon approaching the glass transition, which is a property of fragile liquids.[11] This peculiarity is probably related to the presence of hydrogen bonds.[12] Actually, molecular rearrangements that take place upon cooling the system are hindered, as they involve the breaking of hydrogen bonds. Among alcohols, methanol is the one with the simplest molecular structure. It can be easily converted into a glass in the laboratory, the glass transition temperature being 103 K.[13] In addition, it has been studied by using simulation techniques, and some dynamic correlations as well as the nature of the hydrogen-bonded network in the supercooled state have been previously characterized.[14]

The main goal of our work is to analyze the influence of hydrogen bonding on the properties of supercooled methanol. This system will be simulated by using the molecular dynamics (MD) technique. Results will be compared with those obtained for a nonassociated model polar solvent whose molecules have the same polarity as methanol but that lack sites for hydrogen bonding. Then, both liquids differ only in their ability to establish hydrogen bonds. Thermodynamic, structural, and dynamical properties will be analyzed in both systems to investigate whether they depend on the existence of hydrogen bonding. Our results will be compared with those predicted by MCT. Issues such as the coupling between translational and rotational dynamics and the existence of dynamical heterogeneities will also be addressed.

The paper is organized as follows: In section 2, the models and technical details of the simulations are presented. Thermodynamic and structural results are gathered in sections 3 and 4, respectively. Section 5 is devoted to the results obtained for the dynamical properties, including velocity autocorrelation functions, diffusion coefficients, self-intermediate scattering functions, reorientational dynamics, and van Hove functions. The final section contains some concluding remarks.

2. Models and Simulation Details

Liquid and supercooled methanol (MeOH) have been studied at a wide range of temperatures using the MD technique. The MeOH molecules consist of three beads which represent the methyl group (Me) and the oxygen (O) and hydrogen (H) atoms of the hydroxyl group. The beads are connected through rigid bonds. The intermolecular interactions have been evaluated using the Jorgensen OPLS potential,[15] which consists of a short-range Lennard-Jones part and an electrostatic term. Thermodynamic and structural properties obtained when considering

* E-mail:gemma.sese@upc.es.

10.1021/jp047025v CCC: $30.25
Published on Web 12/16/2004

TABLE 1: Potential Energy (E_p), Enthalpy (H), and Specific Heat(C_P) for Methanol at Several Temperatures

T (K)	E_p (kcal/mol)	H (kcal/mol)	C_P (kcal/(mol K)
298	−8.524	−6.333	0.0204
268	−8.936	−6.934	0.0197
238	−9.326	−7.516	0.0201
218	−9.609	−7.927	0.0187
208	−9.723	−8.104	0.0172
198	−9.828	−8.271	0.0164
178	−10.022	−8.589	0.0168
158	−10.251	−8.944	0.0187

this potential satisfactorily agree with experimental measurements on liquid methanol.[16] The behavior of an ideal system whose molecules have the same dipole moment as methanol but lack sites for hydrogen bonding has also been analyzed. This system will be addressed as MeO because its molecules have only two interacting sites, corresponding to Me and O. The MeO molecular mass is about 3% lower than that of the MeOH molecules. The charges associated to these sites have been chosen so that the molecular dipole equals that of MeOH, given that the molecular neutrality is maintained.

The short-range intermolecular potential used in MeO is the same as that in the MeOH system. This molecular model has already been considered in ref 17. Bond lengths have been constrained in both systems by means of the SHAKE algorithm.[18] The samples under study have been located in cubic boxes with periodic boundary conditions. The Lennard-Jones part of the potential was truncated at one-half of the box length, and the Ewald summation[19] was used to calculate the Coulombic part.

The MeOH sample comprises 216 molecules. Because of the simpler molecular model in the MeO system, simulation of larger samples can be afforded, which will allow reduction of statistical fluctuations. MeO samples consist of 1000 molecules. The integration of the equations of motion has been performed by means of the leapfrog Verlet algorithm, with a time step of 2.5 fs in MeOH and 5 fs in MeO. In an initial (N, V, T) run, the systems were equilibrated at 298 K with a density of 0.787 g/cm^3 in order to determine the pressure, which has been calculated by following ref 20. Values of 1940 and 430 atm have been encountered for MeO and MeOH, respectively. Then, every system was quenched in a stepwise manner with $\Delta T = -5$ K. Every change in the temperature has been followed by a thermalization period of 30 ps. The quenching has been performed in the (N, P, T) ensemble at the pressures previously quoted by using the algorithm proposed by Berendsen et al.[21] Along the cooling process, several temperatures have been selected. Additional equilibration times of 500 and 250 ps for MeOH and MeO, respectively, at the highest temperature, and 1100 and 1750 ps for MeOH and MeO, respectively, at the lowest temperatures, have been considered. Long-term production runs of 275 ps for MeOH and 250 ps for MeO at the highest temperatures and of 3.25 ns for MeOH and 3.75 ns for MeO at the lowest temperature (158 K for MeOH and 103 K for MeO) have been performed in the (N, V, T) ensemble. In this manuscript, the quantities identified with the superscript [′] will correspond to the MeO system.

3. Thermodynamic Properties

The averaged values obtained for the potential energy, the enthalpy, and the specific heat have been gathered in Tables 1 and 2. For both systems, the potential energy decreases upon decreasing the temperature. For all temperatures, the potential energy for the MeOH simulations (E_p) is much lower than that for the MeO ones (E'_p), being approximately $E_p \approx 2.1E'_p$. The energetic differences between them should be associated to the intermolecular hydrogen bonds, which have been supressed in the MeO system. These differences increase only slightly with temperature.

TABLE 2: Potential Energy (E'_p), Enthalpy (H'), and Specific Heat (C'_p) for MeO at Several Temperatures[a]

T	E'_p	E'_{LJ}	E'_{el}	H'	C'_p
298	−3.928	−3.885	−0.043	−0.538	0.0128
268	−4.100	−4.056	−0.044	−0.909	0.0131
238	−4.294	−4.247	−0.047	−1.309	0.0134
218	−4.431	−4.383	−0.048	−1.589	0.0136
208	−4.499	−4.450	−0.049	−1.719	0.0138
198	−4.576	−4.526	−0.050	−1.863	0.0139
178	−4.722	−4.671	−0.051	−2.144	0.0142
158	−4.878	−4.825	−0.053	−2.432	0.0145
138	−5.035	−4.981	−0.054	−2.724	0.0149
123	−5.162	−5.107	−0.055	−2.949	0.0153
103	−5.341	−5.284	−0.057	−3.258	0.0158

[a] The Lennard-Jones (E'_{LJ}) and the electrostatic (E'_{el}) parts of the potential energy are also shown. The units are the same as in Table 1.

As shown in Table 2, the main contribution to E'_p comes from the Lennard-Jones interactions (E'_{LJ}), with the electrostatic contribution (E'_{el}) being about 1% of E'_p. This is consistent with some previous results that showed no structural differences were observed when the charges of the sites in the MeO molecules were neglected.[17] Then, from the thermodynamic point of view, the MeO system behaves basically as a set of rigid diatomic Lennard-Jones molecules. On the contrary, Coulombic interactions are crucial in the properties of MeOH, where the electrostatic part represents more than 90% of the total potential energy. As for the temperature dependence, its relevance decreases weakly on cooling the system, in agreement with ref 22. It is observed that $E_{LJ} \approx 0.082E_p$ at 298 K and $E_{LJ} \approx 0.098E_p$ at 158 K. On the contrary, $E'_{LJ} \approx 0.989E'_p$ in MeO for all temperatures.

The dependence of the total potential energy on temperature has also been analyzed. It has been found in MeO that $E'_p \propto T^n$ with $n = 0.58$. For a Lennard-Jones liquid, $n = 0.6$ both in theoretical studies[23] and MD simulations.[24] This result was obtained in our simulations when fitting E'_{LJ} only. For MeOH, it has been found that $E_p \propto T^{1.65}$. Consequently, the temperature dependence of the specific heat $C_P = (\partial H/\partial T)_P$ is markedly different in both systems. Upon cooling, it decreases in MeOH, whereas it increases in MeO.

4. Structural Properties

Radial distribution functions ($g(r)$'s) involving either molecular sites or centers-of-mass (COMs) have been evaluated for both systems. At room temperature, the absence of hydrogen bonds (HBs) produces dramatic changes in the structure of the system at short distances, as was previously observed.[17] The differences are much more important in $g_{com-com}(r)$ and $g_{OO}(r)$, which are displayed in Figures 1 and 2, respectively. In MeOH, the main maxima of both functions take place at shorter distances, and they are much narrower than the ones in MeO. Actually, the $g_{com-com}(r)$ first maxima in MeO split into two narrower ones in MeOH. In addition, the first minima in $g_{OO}(r)$ are closer to zero in MeOH than in MeO, which indicates that the first coordination shell is much more delimited in the system with HBs. Nevertheless, the long-distance behavior of the $g(r)$ functions depends only weakly on the existence of hydrogen bonds. Indeed, as shown in Figure 1, the maxima and minima of the $g_{com-com}(r)$ corresponding to both systems take

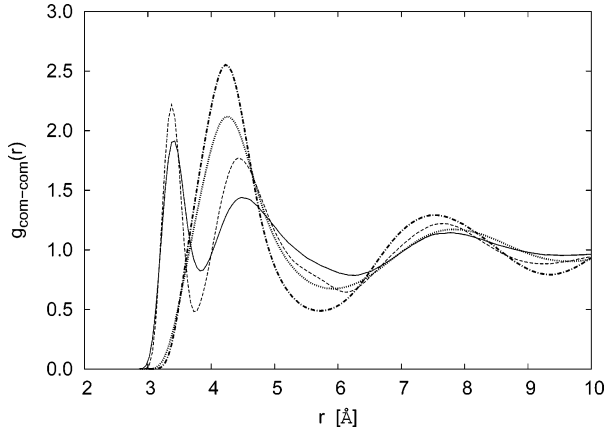

Figure 1. Center-of-mass radial distribution functions for methanol at 298 K (continuous line) and 158 K (dashed line) and for MeO at 298 K (dotted line) and 158 K (dashed−dotted line).

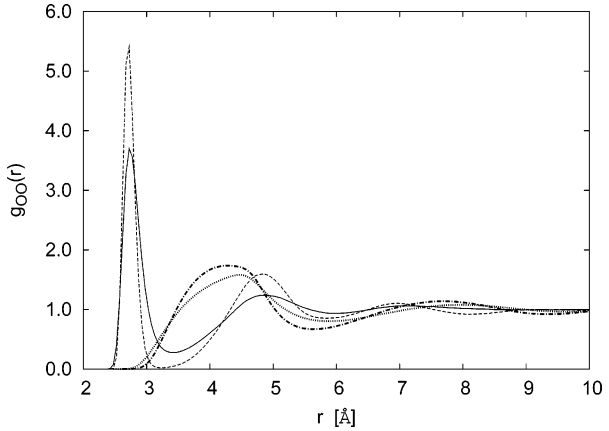

Figure 2. Oxygen−oxygen radial distribution functions for methanol at 298 K (continuous line) and 158 K (dashed line) and for MeO at 298 K (dotted line) and 158 K (dashed−dotted line).

place at approximately the same positions for distances larger than 4.5 Å Decreasing the temperature results in higher maxima and lower minima in both systems, which proves that the nearest- and the next-nearest-neighbor shells become more and more well-defined, as observed in other molecular systems[3]. The positions of the first maxima do not depend on temperature, but the positions of other maxima and minima are slightly shifted toward smaller distances as the samples are cooled.

The coordination number n_1 has been evaluated as

$$n_1 = 4\pi n \int_0^{r_1} r^2 g_{\mathrm{com-com}}(r)\, \mathrm{d}r \qquad (1)$$

where n is the number density and r_1 is the radius of the first coordination shell (i.e., the position of the first minimum of the $g_{\mathrm{com-com}}(r)$). n_1 shows a very weak dependence on temperature in both systems. In MeOH, it has been obtained that $n_1 = 2.1$, which shows that branching is not very important, but a small proportion of MeOH molecules are hydrogen-bonded to more than two molecules at all temperatures, in agreement with ref 14. This HB topology is very similar to the connectivity observed in the methanol crystal structures.[25] When HBs are suppressed, $n_1 = 12$ at 298 K and $n_1 = 13$ at 103 K, results which are consistent with an icosaedral structure in the MeO first shell.

Orientational order has been analyzed in terms of the function $G_1(r)$

$$G_1(r) = \langle P_1[\cos(\theta(r))] \rangle \qquad (2)$$

where P_1 is the first Legendre polynomial and $\theta(r)$ is the angle between the dipole moments of two molecules whose COMs are located at a distance r. The function $G_1(r)$ is shown in Figure 3 for both systems. For all temperatures, the $G_1(r)$ values for the closest MeOH molecules are positive, which corresponds to a parallel orientation. However, $G_1(r)$ values for the closest MeO molecules are negative. This indicates that the orientation tends to be antiparallel. Nevertheless, $G_1(r)$ for MeO also takes positive values at distances corresponding to the first solvation shell. Then, orientation between dipole moments of neighboring molecules is much less restricted in the system without HBs. The results also show that orientational correlations decrease very rapidly with increasing distances for both systems. When temperature decreases, orientation at short distances remains basically unchanged in both systems.

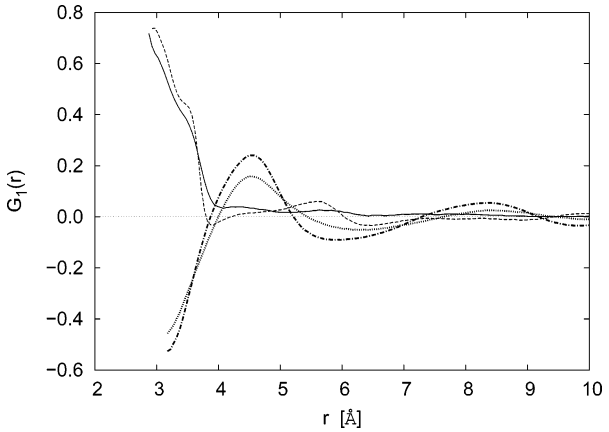

Figure 3. Orientational order $G_1(r)$, defined by eq 2 for methanol at 298 K (continuous line) and 158 K (dashed line) and for MeO at 298 K (dotted line) and 158 K (dashed−dotted line).

5. Dynamical Properties

5.1. Spectra of the Velocity Autocorrelation Functions. Velocity autocorrelation functions $\phi(t)$'s have been evaluated for every interacting site and also for the molecular COM. It has been obtained at room temperature that suppression of HBs results in a slowing down of the initial decay of all $\phi(t)$'s and also in a reduction of some of their characteristic frequencies.[17] This issue has been analyzed by calculating $\phi(\omega)$, the Fourier transforms of $\phi(t)$. The ones corresponding to the COMs for both systems at selected temperatures have been displayed in Figure 4.

All $\phi(\omega)$'s display one maximum at low frequencies, as in most dense liquids. These maxima and the nonvanishing $\phi(0)$ values indicate that molecular motions may be considered as combinations of both temporary vibrations of a tagged molecule inside the cage formed by its neighbors and the diffusive translational motions typical of liquids. Upon cooling, the main peaks shift toward higher frequencies, the shifts in MeO being larger. For all temperatures, a shoulder appears at even higher frequencies in MeOH, but not in MeO. This shoulder is related to the oscillatory behavior of $\phi(t)$, and it is considered as a signature of hydrogen-bonded liquids. It has also been found in water[26,27] and ethanol,[28] but it does not appear in the $\phi(\omega)$ corresponding to non-hydrogen-bonded molecules in methanol.[29] It has also been observed in other systems such as HF,[30] and it can be associated with stretching intermolecular vibrations of hydrogen-bonded molecules. This shoulder takes place at the Einstein's frequency of the system, which can be evaluated from the coefficient corresponding to the quadratic term of a short-term expansion of the $\phi(t)$.[31] This shoulder becomes a secondary peak upon cooling the sample. The Einstein's frequencies at

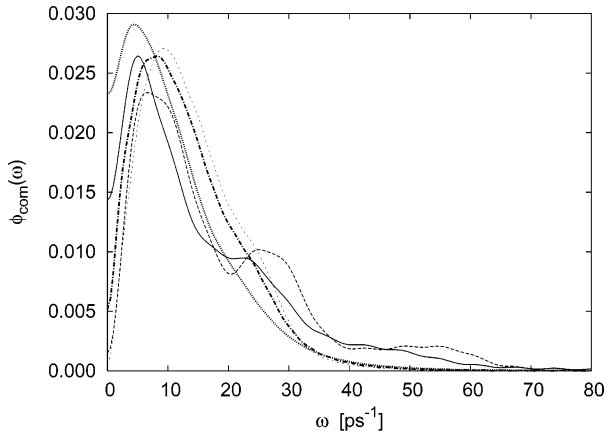

Figure 4. Fourier transforms of center-of-mass velocity autocorrelation functions for methanol at 298 K (continuous line) and 158 K (dashed line) and for MeO at 298 K (dotted line), 158 K (dashed−dotted line), and 103 K (short-dashed line).

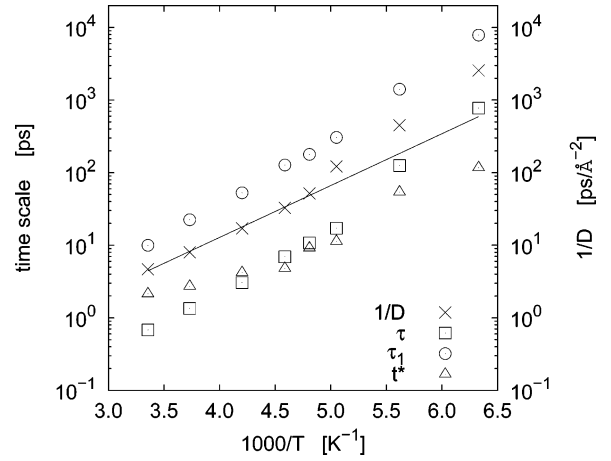

Figure 5. Characteristic times for methanol vs the inverse of temperature: α-relaxation times τ (□) and τ_1 (○). Also included are t^* (△), times corresponding to the maxima of the non-Gaussian parameter, and the inverse of the diffusion coefficients D (×). The solid line corresponds to an Arrhenius-like fit to $1/D$.

298 K for MeOH (Ω_o) and MeO (Ω'_o) are 22.3 and 15.0 ps^{-1}, respectively. Even though Ω_o slightly increases upon cooling, it shows a very weak dependence on temperature in both systems. Their values at the lowest temperatures under study are 25.0 ps^{-1} for MeOH (at 158 K) and 16.4 ps^{-1} for MeO (at 103 K).

For MeO, a very weak shoulder appears at the lowest analyzed temperature at about 25 ps^{-1}. In MeOH, $\phi(\omega)$ displays a band centered at about 50 ps^{-1} at very low temperatures. Both features are probably related to the so-called cage effect and correspond to the oscillatory motion performed by molecules in their next-neighbors' shells.

5.2. Self-Diffusion Coefficients and Mean-Square Displacements. Self-diffusion coefficients (Ds) have been evaluated from the slope of the mean-square displacement by using the Einstein relation[31]

$$D = \lim_{t\to\infty} \frac{\langle r^2(t)\rangle}{6t} \tag{3}$$

For $T > T_A$, D follows an Arrhenius law ($D(T) = A\exp(-E/(k_BT))$. To better appreciate this, $1/D$ has been plotted against $1/T$ in Figures 5 and 6 for MeOH and MeO, respectively. The breakup of the Arrhenius behavior takes place at $T_A \approx 210$

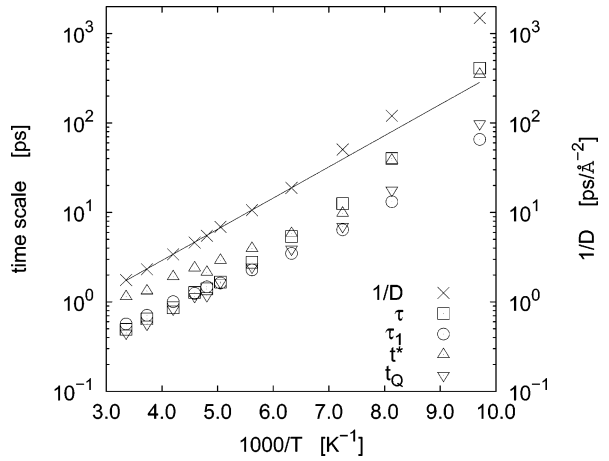

Figure 6. Characteristic times for MeO vs the inverse of temperature: α-relaxation times τ (□) and τ_1 (○). Also included are t^* (△), at which take place the maxima of the non-Gaussian parameter, t_Q (▽), times corresponding to the minima of the $Q(t)$ function (eq 8), and the inverse of the diffusion coefficients D (×). The solid line corresponds to an Arrhenius-like fit to $1/D$.

K for MeOH and at $T'_A \approx 140$ K for MeO. The associated activation energy is much larger in MeOH. It has been found that $E' = 1.595$ kcal/mol and that $E \approx 2E'$. The Arrhenius law overestimates D for $T < T_A$, and their dependence on temperature is better reproduced by a Vogel−Fulcher−Tammann law

$$D = D_o \exp\left(\frac{-B}{T - T_o}\right) \tag{4}$$

The parameters obtained from the fit to eq 4 are $T'_o = 50$ K and $(B/T_o)' = 8.9$ for MeO. For MeOH, $T_o = 72$ K and $B/T_o = 12.5$. Fits to data obtained from diffusion coefficient measurements[32] and dielectric relaxation experiments[33] found that $B/T_o \approx 13$. As for the T_o value obtained for MeOH, it is lower than the one reported in ref 14, but very close to those obtained from experiment.[32,33]

The temperature dependence of D is also consistent with the ideal MCT predictions in both systems. Fits to the function $D \propto (T - T_c)^\gamma$ lead to the values of $T'_c = 94$ K and $\gamma' = 2.18$ for MeO and of $T_c = 133$ K and $\gamma = 3.46$ for MeOH. A critical temperature of 135 K was obtained from a fit to the experimental viscosity of methanol.[34]

To get information about the anisotropy of the molecular motion, the mean-square displacement of the MeO molecule in the direction of the molecular dipole moment and the one perpendicular to it have been calculated separately. For this purpose, at a time t_0, three directions have been defined for each molecule, namely ($\hat{l}$, $\hat{t}_1$, $\hat{t}_2$). $\hat{l}$ is a unit vector in the direction of the molecular dipole moment, and $\hat{t}_1$ and $\hat{t}_2$ are orthonormal to $\hat{l}$. At a time t, the COM displacement vector of a MeO molecule can be written as

$$\boldsymbol{r}(t) - \boldsymbol{r}(t_0) = r_l\hat{l} + r_{t1}\hat{t}_1 + r_{t2}\hat{t}_2 \tag{5}$$

with r_l being the projection of the displacement vector onto the initial molecular dipole direction $\hat{l}$. r_{t1} and r_{t2} are the projections onto the directions $\hat{t}_1$ and $\hat{t}_2$, respectively. The square modulus of eq 5 can be written as

$$|\boldsymbol{r}(t) - \boldsymbol{r}(t_0)|^2 = r_l^2 + r_{t1}^2 + r_{t2}^2 = r_l^2 + r_t^2 \tag{6}$$

After averaging over all molecules and over several time origins, it is possible to obtain the mean-square displacement in the

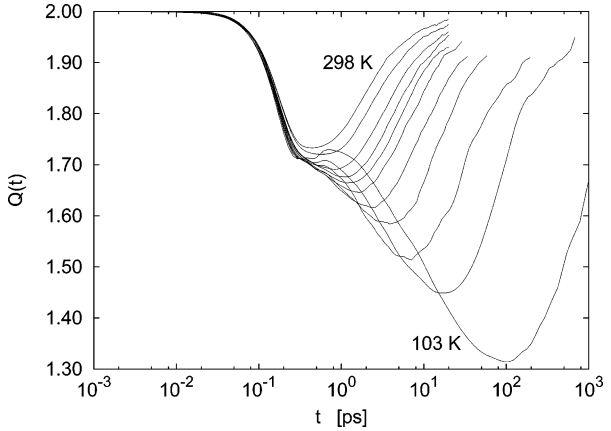

Figure 7. $Q(t)$ defined by eq 8 for MeO at 298, 268, 238, 218, 208, 198, 178, 158, 138, 123, and 103 K.

direction of the molecular dipole ($\langle r_l^2(t)\rangle$) and the one onto the plane perpendicular to this direction ($\langle r_t^2(t)\rangle$) according to

$$\langle r^2(t)\rangle = \langle |\mathbf{r}(t) - \mathrm{r}(t_0)|^2\rangle = \langle r_l^2(t)\rangle + \langle r_t^2(t)\rangle \qquad (7)$$

To analyze the relevance of this two terms, the function $Q(t)$ is defined as

$$Q(t) = \frac{\langle r_t^2(t)\rangle}{\langle r_l^2(t)\rangle} \qquad (8)$$

Function $Q(t)$ is displayed in Figure 7. For all temperatures, it initially decreases, reaches a minimum at t'_Q, which depends very much on temperature, and then increases. The result $Q = 2$ is consistent with an isotropic dynamics ($\langle r_t^2(t)\rangle = 2\langle r_l^2(t)\rangle$). The initial decay ($0.03 < t < 0.2$ ps) does not depend on temperature. During this period, a molecule tends to move in the dipole direction. This effect completely disappears in the hydrodynamic regime, that is, for $t \rightarrow \infty$, where the dynamics is completely isotropic. This regime is reached earlier at higher temperatures. At very low temperatures, a different regime appears for $0.2 \text{ ps} < t < t_m$, with $1 < t_m < 100$ ps, t_m becoming larger upon lowering the temperature. During this time interval, the decay is much slower than the initial one, but the dynamics is still clearly anysotropic. The so-called β-relaxation regime takes place during this time interval, as will be shown in the following section. $Q(t)$ reaches a minimum at t'_Q, which can be fitted to a critical law

$$t'_Q \propto (T - T_c)^{-\gamma} \qquad (9)$$

with $T_c = 90$ K and $\gamma = 1.97$.

5.3. Self-Intermediate Scattering Functions. The self-intermediate scattering function of COM has been evaluated by following

$$F_s(k, t) = \langle \exp(i\mathbf{k}[\mathbf{r}_i(t) - \mathbf{r}_i(0)])\rangle \qquad (10)$$

where $\mathbf{k}$ is the wavenumber, compatible with the periodic boundary conditions. $F_s(k, t)$ values have been calculated for both systems at $k = k_{max}$, which is the wavenumber at which the structure factor $S(k)$ displays a maximum. For both systems, $k_{max} = 1.8$ Å^{-1}, which implies the existence of structural similarities between them. Indeed, the characteristic length associated to this wavenumber corresponds to the distance between the second and third maxima of $g_{com-com}(r)$ in MeOH but also to the distance between the first and second maxima

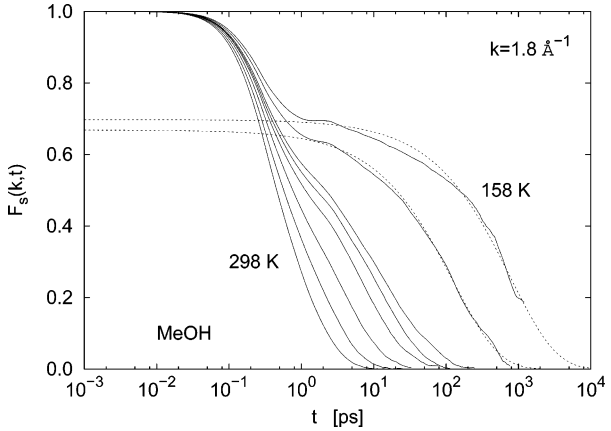

Figure 8. $F_s(k, t)$ for methanol at 298, 268, 238, 218, 208, 198, 178, and 158 K. Fits to eq 11 for the two lowest temperatures are also displayed (dashed lines).

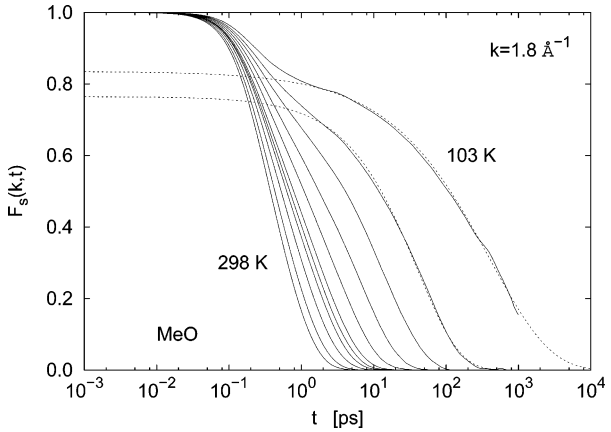

Figure 9. $F_s(k, t)$ for MeO at 298, 268, 238, 218, 208, 198, 178, 158, 138, 123, and 103 K. Fits to eq 11 for the two lowest temperatures are also displayed (dashed lines).

of the same function in MeO, as shown in Figure 1. Then, the local structure at those distances is almost independent of the existence of HB.

$F_s(k, t)$ functions have been displayed in Figures 8 and 9 for MeOH and MeO, respectively. For all temperatures, $F_s(k, t)$ functions present a short time decay, which corresponds to the ballistic regime, and a slow decay to zero for long times, the so-called α-relaxation regime. Between them, a shoulder appears upon cooling, which becomes a quasiplateau at very low temperatures. It corresponds to the β-relaxation regime predicted by MCT. It should be noted that the early part of the α-relaxation coincides with the late part of the β-relaxation. In contrast with our findings, the authors of some previous supercooled methanol simulations[14] claimed that it was not possible to identify distinct α- and β-relaxation regimes in their results. They also obtained different potential energies and critical temperatures. Their potential parameters are different from ours. In additon, differences in the considered cooling rates might contribute to these discrepancies.[35]

In the α-relaxation zone, $F_s(k, t)$ can be fitted to a stretched exponential

$$F_s(k, t) = A \exp\left[-\left(\frac{t}{\tau}\right)^{\beta}\right] \qquad (11)$$

τ is the time scale corresponding to the α-relaxation. The fits performed on the simulation curves are good, especially for long times, as shown in Figures 8 and 9. The τ values for both

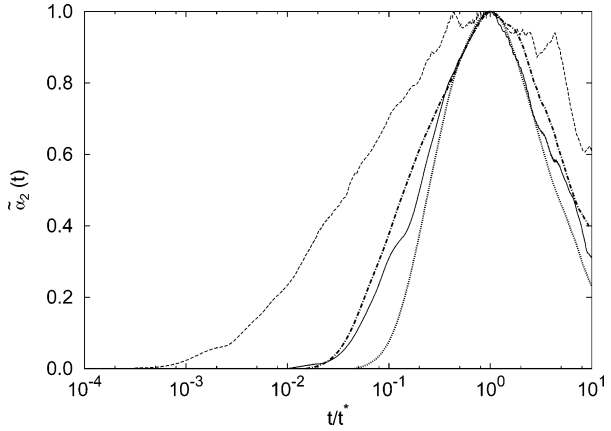

Figure 10. Normalized non-Gaussian parameter $\tilde{\alpha}_2(t)$ (eq 13) vs t/t^* for methanol at 298 K (continuous line) and 158 K (dashed line) and for MeO at 298 K (dotted line) and 158 K (dashed−dotted line).

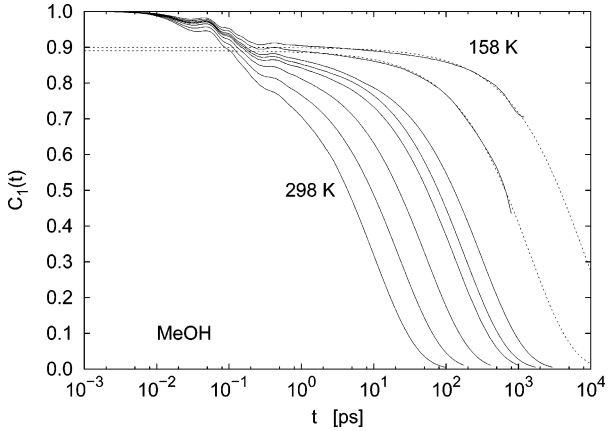

Figure 11. $C_1(t)$ (eq 14) for methanol at 298, 268, 238, 218, 208, 198, 178, and 158 K. Fits to eq 11 for the two lowest temperatures are also displayed (dashed lines).

systems are plotted in Figures 5 and 6 against $1/T$. It is apparent that the values corresponding to MeOH are larger than those for MeO. τ can be fitted to a critical law (eq 9) predicted by MCT. For MeOH, $T_c = 134$ K and $\gamma = 3.77$, and for MeO, $T_c' = 94$ K and $\gamma' = 2.22$, which are very close to the values obtained when fitting D, especially for the non-HB system.

$F_s(k, t)$ can be approximated by a Gaussian distribution both in the free-particle regime and in the hydrodynamic limit. The deviations from this Gaussian behavior can be analyzed by means of the first non-Gaussian parameter $\alpha_2(t)$, defined as[36]

$$\alpha_2(t) = \frac{3\langle r^4(t)\rangle}{5\langle r^2(t)\rangle^2} - 1 \tag{12}$$

This function always goes to zero for $t \rightarrow 0$ and $t \rightarrow \infty$, and it reaches a maximum at an intermediate time t^*, which correlates with the onset of the α-relaxation. The t^* values have been plotted against $1/T$ in Figures 5 and 6 for MeO and MeOH, respectively. At room temperature, t^* in MeOH is almost twice that in MeO. On cooling, t^* increases in both systems. We can also compare t^* with τ, the $F_s(k, t)$ characteristic time. At high temperatures, $\tau < t^*$, whereas $\tau > t^*$ at low temperatures for both systems. It is apparent in the plots that $\tau = t^*$ at about T_A, the breakup temperature of the Arrhenius behavior for D in each system.

$\alpha_2(t^*)$ takes bigger values in MeOH than in MeO at all temperatures, which indicates that the non-Gaussian behavior is less important when HBs are suppressed. The normalized non-Gaussian functions have been evaluated as

$$\tilde{\alpha}_2(t) = \frac{\alpha_2(t/t^*)}{\alpha_2(t^*)} \tag{13}$$

$\tilde{\alpha}_2(t)$ versus t/t^* are displayed in Figure 10 for both systems at two different temperatures. It is apparent that for $t < t^*$, $\tilde{\alpha}_2(t)$ is always bigger in MeOH. But, during the so-called α-relaxation regime (for $t > t^*$), the curves corresponding to both systems fall quite well onto the same master curve. Then, the long-term behavior of this function does not depend on the existence of HBs.

5.4. Reorientational Dynamics. The reorientational dynamics has been analyzed by means of the correlation function $C_1(t)$

$$C_1(t) = \left\langle P_1\left[\cos\left(\frac{\mu(t)\cdot\mu(0)}{\mu(0)\cdot\mu(0)}\right)\right]\right\rangle \tag{14}$$

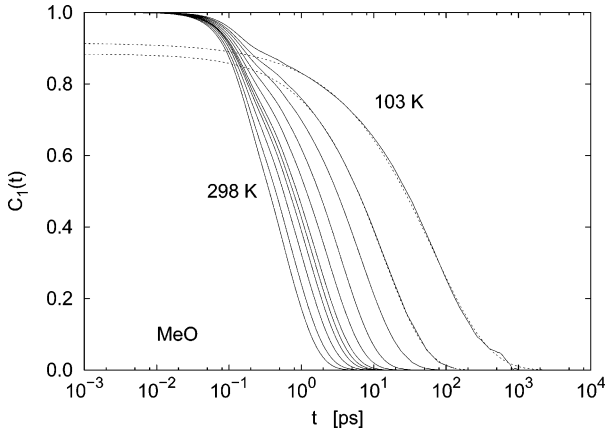

Figure 12. $C_1(t)$ (eq 14) for MeO at 298, 268, 238, 218, 208, 198, 178, 158, 138, 123, and 103 K. Fits to eq 11 for the two lowest temperatures are also displayed (dashed lines).

where P_1 is the first Legendre polynomial and $\mu(t)$ is the molecular dipole vector at time t. The $C_1(t)$ functions have been displayed in Figures 11 and 12 at several temperatures. All $C_1(t)$ functions show a rapid initial decay followed by a nonexponential tail. At very low temperatures, a quasiplateau precedes the long-term relaxation. Only for MeOH, the $C_1(t)$ functions display an oscillatory behavior after the very short monotonic decay. These oscillations have also been observed in other associated molecular liquids,[4,37] and they can be related to librational motions of individual molecules belonging to hydrogen-bonded chains. The last part of all $C_1(t)$'s can be fitted to a stretched exponential function (eq 11). The corresponding time scales τ_1's are displayed against $1/T$ in Figures 5 and 6. They decrease with temperature, and they follow a critical law (eq 9), with critical temperatures of 125 K for MeOH and 92 K for MeO and γ values of 4.06 for MeOH and 1.63 for MeO.

Differences in the temperature dependence of translational diffusion coefficients and rotational relaxation times have been encountered in our systems. The quantity $D\tau_1$ has a weak, although nonzero, dependence on temperature. Upon cooling, it decreases in MeO, whereas it slightly increases in MeOH. Much stronger dependences have been encountered experimentally for other systems,[38] where diffusion is strongly enhanced over rotation at temperatures very close to the glass transition ($T \approx 1.2T_g$). Several explanations, which have been tested in simulations, have been offered to account for this result, as the existence of dynamical heterogeneities[39,40] or the influence of intermolecular cooperativity in the framework of the so-called

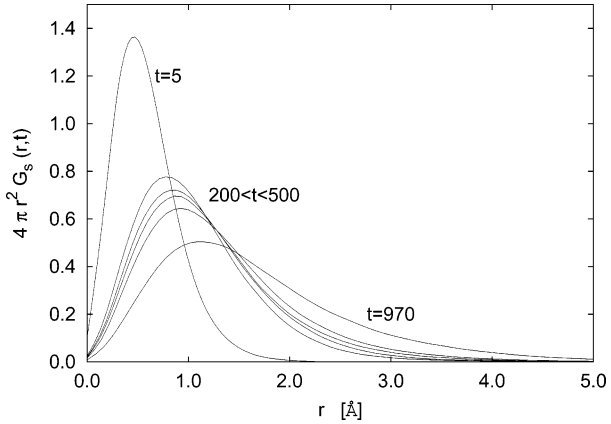

Figure 13. Self part of the van Hove function at 103 K for the observation times displayed in the frame (in picoseconds). For the sake of clarity, only a few functions within the time interval $200 < t < 500$ ps have been drawn.

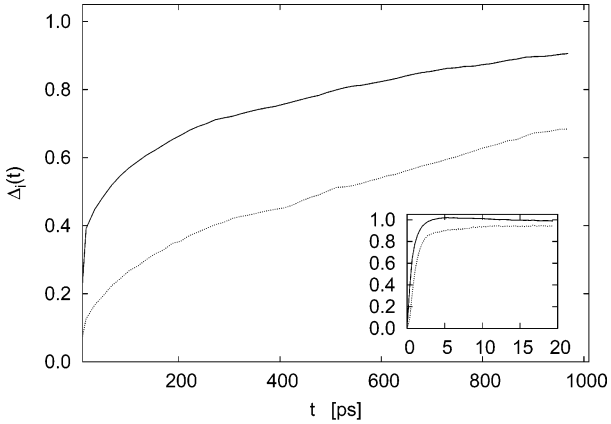

Figure 14. $\Delta_1(t)$ (continuous line) and $\Delta_2(t)$ (dotted line) defined by eq 16 for MeO at 103 K. The same functions at 298 K are displayed in the inset.

coupling model.[41] Nevertheless, the temperatures considered in our MeOH simulations are still too high to identify the temperature dependence of $D\tau_1$ with the so-called diffusion-enhanced phenomenon.[42]

At room temperature, the reorientational characteristic time (τ_1) is much bigger than the translational one (τ) in MeOH ($\tau = 0.07\tau_1$), whereas both characteristic times are of the same order of magnitude in MeO ($\tau' = 0.87\tau'_1$). The translational relaxation time increases at a faster rate than the reorientational relaxation time upon cooling, especially in MeO. At the lowest analyzed temperature, $\tau' = 6.27\tau'_1$ in MeO, whereas $\tau = 0.09\tau_1$ in MeOH. Then, reorientational motions are almost frozen in the deep MeOH supercooled state, but they are still important for the dynamics in MeO. This is probably motivated by the dynamical restrictions imposed by the directionality of intermolecular bonds in methanol, but not in MeO.

5.5. Dynamical Heterogeneities. The van Hove correlation function for the molecular COM is defined as[31]

$$G(\mathbf{r}, t) = \frac{1}{N}\left\langle \sum_i \sum_j \delta[\mathbf{r} + \mathbf{r}_j(0) - \mathbf{r}_i(t)] \right\rangle \qquad (15)$$

where $\mathbf{r}_i$ and $\mathbf{r}_j$ are the positions of the COM of molecules i and j, respectively. $G(\mathbf{r}, t)$ can be separated into *self* ($G_s(\mathbf{r}, t)$) and *distinct* ($G_d(\mathbf{r}, t)$), depending on whether i and j refer to the same molecule or to a different one. For $t = 0$, $G_s(\mathbf{r}, 0) = \delta(\mathbf{r})$ and $G_d(\mathbf{r}, 0) = ng_{com-com}(r)$. On a very long time scale, $G_s(r, \infty) = 1/V \approx 0$ and $G_d(r, \infty) \approx n$.

$G_s(\mathbf{r}, t)$ functions have been evaluated, and similar qualitative results have been obtained in both systems. The functions corresponding to the MeO system for several time intervals at the lowest analyzed temperature are displayed in Figure 13. On very short and very long time scales, they follow a Gaussian distribution.[31] It is remarkable that at intermediate times (for $200 < t < 500$ ps) $G_s(r, t)$ depend only weakly on time, which indicates that molecules basically vibrate inside their nearest-neighbor shells. For MeO, this subdiffusive regime takes place at times between 200 and 500 ps, which corresponds to the β-relaxation regime, already identified in the analysis of $F_s(k_{max}, t)$.

$G_d(\mathbf{r}, t)$ functions have also been evaluated for MeO at several time intervals. They depend very much on temperature. Their asymptotic behavior for large t is reached after 20 ps at room temperature, whereas it takes more than 1000 ps at $T = 103$ K. To further analyze this, we have calculated the functions $\Delta_l(t)$, with $l = 1$ and 2, defined as

$$\Delta_l(t) = \frac{g_{com-com}(r_l) - G_d(r_l, t)/n}{g_{com-com}(r_l) - 1} \qquad (16)$$

where r_1 and r_2 correspond to the positions of the first and second minima of $g_{com-com}(r)$, respectively. These functions give information about the relaxation times associated to the ensemble of molecules located in the first and second coordination shells, respectively. From the behavior of $G_d(r, t)$, it follows that $\Delta_l(0) = 0$ and $\Delta_l(\infty) = 1$. At intermediate times, Δ_l functions increase monotonically, as shown in Figure 14, where they have been displayed at two different temperatures. It is also apparent that $\Delta_1(t)$ tends to reach its asymptotic value more rapidly than $\Delta_2(t)$, especially on a short time scale. By defining t_1 and t_2 so that $\Delta_1(t_1) = \Delta_2(t_2) = 1/2$, it has been found that at room temperature, $t_1 \approx \tau'$, and at 103 K, $t_2 \approx \tau'$. At this very low temperature, diffusion between consecutive shells is very difficult and takes place on very large time scales. It should be noted that $[\langle r^2(t_2)\rangle]^{1/2} = 1.71$ Å, whereas $r_2 = 7.3$ Å. Moreover, when $\langle r^2(t_2)\rangle$ is evaluated for the fastest 70 molecules in the system (see following text), it is found that $[\langle r^2(t_2)\rangle]^{1/2} = 6.50$ Å. Then, dynamical heterogeneities do exist in the system without HB.

We have considered that a molecule is fast at a given interval t if its displacement r satisfies $r \geq d$, where $d = [\langle r^2(t)\rangle]^{1/2}$. The fraction of fast molecules in the system can be evaluated by following

$$f(t) = \int_d^\infty 4\pi r^2 G_s(r, t)\, dr \qquad (17)$$

If $G_s(\mathbf{r}, t)$ follows a Gaussian distribution, $f = 0.392$. $f(t)$ has been calculated for $t = t^*$, corresponding to the maximum in the non-Gaussian parameter (displayed in Figures 5 and 6) for each analyzed temperature. Maximum heterogeneity is expected at this time interval.[43,44] The $f(t^*)$ values have been displayed in Table 3 for MeO and MeOH. Similar values have been obtained for both systems at room temperature. As temperature decreases, $f(t^*)$ decreases, but this tendency is more important in MeOH. Then, dynamical heterogeneities do exist in both systems, and they are more remarkable in the system with HB. The values for $\alpha_2(t^*)$ have also been gathered in Table 3. It has been found that $f(t^*)$ depends linearly on $\alpha_2(t^*)$ and that the slope of the fit is the same in both systems. This result can be

TABLE 3: Fraction of Fast Molecules (Eq 17) and Maximum Values of the Non-Gaussian Parameters (Eq 12) at Several Temperatures

	methanol		MeO	
T (K)	$f(t^*)$	$\alpha_2(t^*)$	$f'(t^{*\prime})$	$(\alpha_2')(t^{*\prime})$
298	0.347	0.137	0.342	0.080
268	0.342	0.162	0.340	0.088
238	0.336	0.202	0.339	0.100
218	0.325	0.279	0.337	0.112
208	0.321	0.313	0.333	0.113
198	0.317	0.344	0.334	0.124
178	0.287	0.559	0.329	0.149
158	0.262	0.702	0.323	0.176
138			0.315	0.227
123			0.306	0.318
103			0.292	0.393

also obtained analytically by considering only the first term of the $G_s(r, t)$ expansion in the even Hermite polynomials.[36]

Finally, as for its temperature dependence, it has been found that $f(t^*)$ can be fitted to a critical law (eq 9). The associated critical temperature is 148 K for MeOH and 91 K for MeO, which differ from the values obtained for the overall diffusion coefficients by 10% and 3%, respectively. γ_f equals 0.110 for MeOH and 0.059 for MeO. If we assume that the largest contribution to diffusion is that of the fast molecules, $D \approx fD_f$, where D_f is the diffusion coefficient associated to the fast molecules. Then, D_f also follows a critical law with the same critical temperature as that of the overall diffusion coefficient, especially in the nonassociated system.

6. Concluding Remarks

Molecular dynamics simulations have been performed to analyze the effects of the existence of hydrogen bonds (HBs) on thermodynamic, structural, and dynamical properties of supercooled methanol. HBs have been removed by supressing the hydrogen sites in the methanol model, and the charges associated to the remaining sites have been distributed so that the molecules in the non-HB liquid have the same molecular dipolar moment as the methanol molecules. The potential energy of the non-HB system is higher than that of methanol by a factor of 2. Even though electrostatic interactions do exist in both systems, the electrostatic part is about 1% of the total potential energy in the non-HB liquid, whereas it amounts the 99% of the total potential energy in methanol. The dependence of the potential energy on temperature is very different in both systems. As a consequence, the specific heat decreases upon cooling in methanol, whereas it increases in the non-HB system.

Radial distribution functions have been evaluated in both systems. The first coordination shell is much larger in the non-HB system, and it contains 12 next-neighbors, which is characteristic of an icosaedral structure. In methanol, the coordination number is slightly higher than 2, which is consistent with a structure of linear HB chains, with some branching. Upon cooling, radial distribution functions of both systems display higher maxima and lower minima, but the coordination numbers depend very weakly on temperature. This is also true for the preferred orientation of molecular moments of molecules in the first coordination shell. It tends to be parallel in methanol and antiparallel in the non-HB system at all temperatures, even though the orientation in the latter is less restricted.

The center-of-mass spectra have also been analyzed. At room temperature, they display a first peak located at very low frequencies. A shoulder appears at higher frequencies in methanol only, which is a signature of the existence of HBs. Upon cooling, the main peaks shift toward higher frequencies in both systems, the shoulder becomes a peak in methanol, and at the same frequency, a very weak shoulder appears in the non-HB system at very low temperatures. This should be associated to the vibrations of molecules in their nearest neighbors' shells, the so-called *cage effect* that appears at very low temperatures. The existence of a band centered at higher frequencies should also be associated to this effect in methanol.

Translation and reorientational dynamics have been studied at a wide range of temperatures, and the results show a good agreement with the predictions of the mode-coupling theory in both systems. It has been found that translation is not isotropic in the non-HB system. For the initial time steps, the ballistic regime, molecules tend to move in the dipole moment direction, and this tendency is maintained till the end of the β-relaxation regime. An isotropic motion is reached only at the end of the α-regime.

Characteristic relaxation times can be fitted to temperature-dependent critical laws in both systems. The critical temperatures associated to diffusion and translation differ by less than 1%, and the ones associated to different relaxation times differ by less than 5%. Suppression of HBs results in lower values for the critical temperatures.

Upon cooling the methanol samples, translational relaxation times increase more rapidly than reorientational ones. This effect is much more important when hydrogen bonds are suppressed. At temperatures close to the critical one, translational motions are frozen in both systems. Reorientational dynamics is virtually stopped in methanol, whereas it is still relevant when HBs are suppressed.

Signatures of dynamical heterogeneities have been found independently of the existence of HBs. A preliminary study performed in the nonassociated liquid reveals that there is a heterogeneous distribution of local relaxation times. Further analyses of the correlation between dynamical and spatial heterogeneities in these systems are in progress.

Acknowledgment. The authors are indebted to Prof. Walter Kob, Dr. Manel Canales, and Prof. Joan A. Padró for interesting discussions and a careful reading of the manuscript. Financial support of DGICYT (project BFM2000-0596-C03-02) and of Generalitat de Catalunya (project 2001SGR 00222) is acknowledged.

References and Notes

(1) Kob, W. *J. Phys.: Condens. Matter* **1999**, *11*, R85.
(2) Lewis, L. J.; Wahnström, G. *Phys. Rev. E* **1994**, *50*, 3865.
(3) Sciortino, F.; Gallo, P.; Tartaglia, P.; Chen, S. H. *Phys. Rev. E* **1996**, *54*, 6331.
(4) Sesé, G.; Palomar, R. *J. Chem. Phys.* **2001**, *114*, 9974.
(5) Bengtzelius, U.; Götze, W.; Sjölander, A. *J. Phys. C: Solid State Phys.* **1984**, *17*, 5915.
(6) Götze, W. In *Liquids, Freezing and the Glass Transition*; Hansen, J. P., Levesque, D., Zinn-Justin, J., Eds.; Les Houches, Session LI, 1989; North-Holland: Amsterdam, 1991.
(7) Kob, W. In *Supercooled liquids: Advances and Novel Applications*; Fourkas, J. T., Kivelson, D., Mohanty, U., Nelson, K. A., Eds.; ACS Symposium Series 676; American Chemical Society: Washington, DC, 1997; p 28.
(8) Gleim, T.; Kob, W.; Binder, K. *Phys. Rev. Lett.* **1998**, *81*, 4404.
(9) Bordat, P.; Affouard, F.; Descamps, M.; Ngai, K. L. *Phys. Rev. Lett.* **2004**, *93*, 105502.
(10) Ediger, M. D. *Annu. Rev. Phys. Chem.* **2000**, *51*, 99.
(11) Angell, C. A. *J. Non-Cryst. Solids* **1991**, *131*−*133*, 13.
(12) Alba-Simionesco, C.; Fan, J.; Angell, C. A. *J. Chem. Phys.* **1999**, *110*, 5262.
(13) Sugisaki, M.; Sugaand, H.; Seki, S. *Bull. Chem. Soc. Jpn.* **1968**, *41*, 2586.
(14) Sindzingre, P.; Klein, M. L. *J. Chem. Phys.* **1992**, *96*, 4681.
(15) Jorgensen, W. L. *J. Phys. Chem.* **1986**, *90*, 1276.

(16) Haughney, M.; Ferrario, M.; McDonald, I. R. *J. Phys. Chem.* **1987**, *91*, 4934.
(17) Guárdia, E.; Sesé, G.; Padró, J. A. *J. Mol. Liq.* **1994**, *62*, 1.
(18) Ryckaert, J. P.; Cicotti, G.; Berendsen, H. J. C. *J. Comput. Phys.* **1999**, *23*, 327.
(19) Allen, M. P.; Tildesley, D. J. *Computer Simulation of Liquids*; Clarendon Press: Oxford, 1987.
(20) Hummer, G.; Gronbech-Jensen, N.; Neumann, M. *J. Chem. Phys.* **1998**, *109*, 2791.
(21) Berendsen, H. J. C.; Postma, J. P. M.; van Gunsteren, W. F.; DiNola, A.; Haak, J. R. *J. Chem. Phys.* **1984**, *81*, 3684.
(22) Kabeya, T.; Tamain, Y.; Tanaka, H. *J. Phys. Chem. B* **1998**, *102*, 5.
(23) Rosenfeld, Y.; Tarazona, P. *Mol. Phys.* **1998**, *95*, 141.
(24) Sciortino, F.; Kob, W.; Tartaglia, P. *J. Phys.: Condens. Matter* **2000**, *12*, 6525.
(25) Tauer, K. J.; Lipscomb, W. N. *Acta Crystallogr.* **1952**, *5*, 606.
(26) Martí, J.; Padró, J. A.; Guárdia, E. *J. Chem. Phys.* **1996**, *105*, 639.
(27) Balucani, U.; Brodholt, J. P.; Vallauri, R. *J. Phys.: Condens. Matter* **1996**, *8*, 6139.
(28) Saiz, L.; Padró, J. A.; Guárdia, E. *J. Phys. Chem. B* **1997**, *101*, 78.
(29) Martí, J.; Padró, J. A.; Guárdia, E. *J. Mol. Liq.* **1995**, *64*, 1.
(30) Balucani, U.; Bertolini, D.; Stumann, G.; Tani, A.; Vallauri, R. *J. Chem. Phys.* **1999**, *111*, 4663. 31. Hansen, J. P.; McDonald, I. R. *Theory of simple liquids*; Academic Press: London, 1986.
(31) Karger, N.; Vardag, T.; Ludemann, H. D. *J. Chem. Phys.* **1990**, *93*, 3437.
(32) Angell, C. A.; Smith, D. L. *J. Phys. Chem.* **1982**, *86*, 3845.
(33) Taborek, P.; Kleiman, R. N.; Bishop, D. J. *Phys. Rev. B* **1986**, *34*, 1835.
(34) Vollmayr, K.; Kob, W.; Binder, K *J. Chem. Phys.* **1996**, *105*, 4714.
(35) Rahman, A. *Phys. Rev.* **1964**, *136*, A405. 37. Fabbian, L.; Sciortino, F.; Tartaglia, P. *J. Non-Cryst. Solids* **1998**, *235*−*237*, 325.
(36) Cicerone, M. T.; Ediger, M. D. *J. Chem. Phys.* **1996**, *104*, 7210.
(37) Cicerone, M. T.; Wagner, P. A.; Ediger, M. D. *J. Phys. Chem. B* **1997**, *101*, 8727.
(38) Bhattacharyya, S.; Mukherjee, A.; Bagchi, B. *J. Chem. Phys.* **2002**, *117*, 2741.
(39) Ngai, K. L. *J. Phys. Chem. B* **1999**, *103*, 10684.
(40) Ngai, K. L.; Magill, J. H.; Plazek, D. J. *J. Chem. Phys.* **2000**, *112*, 1887.
(41) Doliwa, B.; Heuer, A. *cond-mat/9902177*. http://arxiv.org/PS_cache/cond-mat/pdf/9902/9902177.pdf
(42) Kob, W.; Donati, C.; Plimpton, S. J.; Poole, P. H.; Glotzer, S. C. *Phys. Rev. Lett.* **1997**, *79*, 2827.